

Competing phases in the room-temperature  
 $M_2(2,6\text{-ndc})_2(\text{dabco})$  metal–organic framework thin film  
synthesis

Supporting Information

Lucile Hamon,<sup>1</sup> Iryna Andrusenko,<sup>2</sup> Aurelio Borzì,<sup>1</sup> Michael Stiefel,<sup>3</sup> Stephan Carl,<sup>4</sup> Ruggero Frison,<sup>1</sup> Antonio Cervellino,<sup>5</sup> Mauro Gemmi,<sup>2</sup> Gustavo Santiso-Quinones,<sup>6</sup> Eric Hovestreydt,<sup>6</sup> Antonia Neels,<sup>1</sup> and Ines E. Collings<sup>1,\*</sup>

<sup>1</sup>Center for X-ray Analytics, Swiss Federal Laboratories for Materials Science and Technology, Überlandstrasse 129, 8600 Dübendorf, Switzerland.

<sup>2</sup>Istituto Italiano di Tecnologia, Center for Materials Interfaces, Electron Crystallography, Viale Rinaldo Piaggio 34, 56025 Pontedera (PI), Italy

<sup>3</sup>Transport at Nanoscale Interfaces, Swiss Federal Laboratories for Materials Science and Technology, Überlandstrasse 129, 8600 Dübendorf, Switzerland.

<sup>4</sup>Laboratory of Multiscale Studies in Building Physics, Swiss Federal Laboratories for Materials Science and Technology, Überlandstrasse 129, 8600 Dübendorf, Switzerland.

<sup>5</sup>Laboratory for Synchrotron Radiation – Condensed Matter,  
Paul Scherrer Institute, 5232 Villigen, Switzerland

<sup>6</sup>ELDICO Scientific AG, 5232 Villigen, Switzerland

\*E-mail: collings.ie@gmail.com

## Contents

<b>1 Bulk synthesis</b>	<b>S3</b>
1.1 Cu <sub>2</sub> (2,6-ndc) <sub>2</sub> dabco . . . . .	S3
1.2 Zn <sub>2</sub> (2,6-ndc) <sub>2</sub> dabco . . . . .	S3
1.3 Ni <sub>2</sub> (2,6-ndc) <sub>2</sub> dabco . . . . .	S6
<b>2 3D electron diffraction</b>	<b>S7</b>
2.1 Zn(2,6-ndc)(H <sub>2</sub> O) . . . . .	S7
2.2 Cu(2,6-ndc) . . . . .	S11
<b>3 Thin films</b>	<b>S12</b>
3.1 M=Zn, SAM=MHDA . . . . .	S15
3.2 M=Zn, SAM=4-PyS . . . . .	S16
3.3 M=Zn, SAM=none . . . . .	S17
3.4 M=Cu, SAM=MHDA . . . . .	S18
3.5 M=Cu, SAM=4-PyS . . . . .	S22
3.6 M=Cu, SAM=none . . . . .	S23
3.7 SEM thin film cross section . . . . .	S24

# 1 Bulk synthesis

## 1.1 Cu<sub>2</sub>(2,6-ndc)<sub>2</sub>dabco

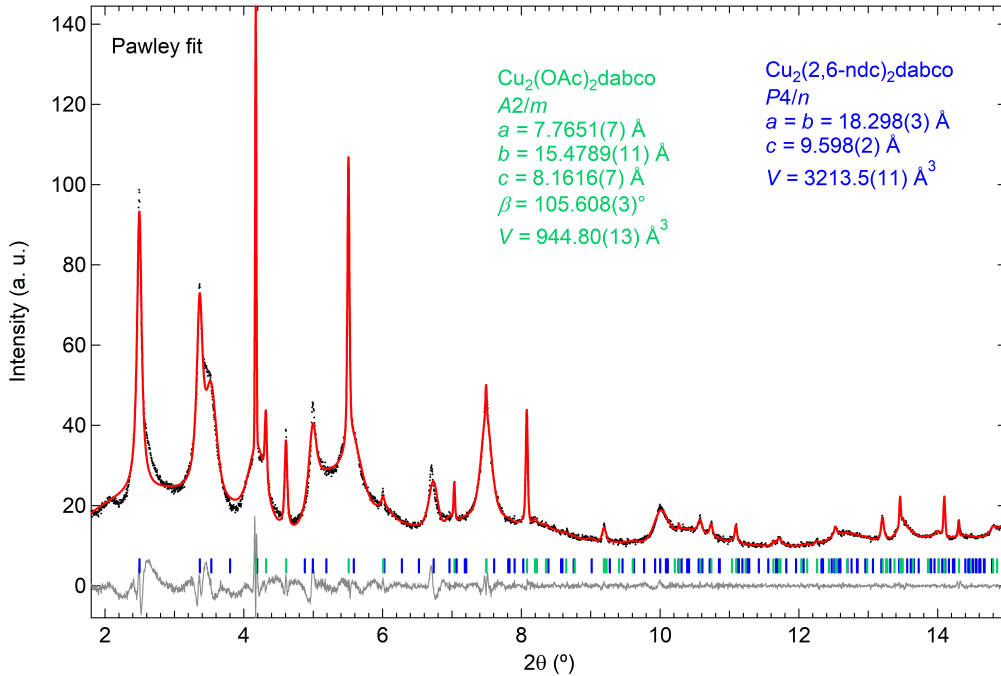


Figure S1: Pawley refinement of the synchrotron X-ray powder diffraction measured on the ambient powder synthesis of Cu<sub>2</sub>(2,6-ndc)<sub>2</sub>dabco, exhibiting a phase mixture of Cu<sub>2</sub>(OAc)<sub>2</sub>dabco and Cu<sub>2</sub>(2,6-ndc)<sub>2</sub>dabco, where OAc=acetate.

## 1.2 Zn<sub>2</sub>(2,6-ndc)<sub>2</sub>dabco

The targeted synthesis of Zn<sub>2</sub>(2,6-ndc)<sub>2</sub>dabco at ambient conditions could not be verified from the X-ray powder diffraction. The published  $P2/n$  and  $C2/m$  structural models were used to refine the data,<sup>S1, S2</sup> however, these fits resulted in large changes to the unit cell dimensions, resulting in unphysical Zn–O bonding distances. Moreover, the sample was not stable with time [Figure S2].

Growth of targeted Zn<sub>2</sub>(2,6-ndc)<sub>2</sub>(dabco) in ethanol solution with a few drops of acetic acid resulted in the formation of the co-crystals of 2,6-ndc:dabco. Initial indexing of the single-crystal diffraction data gives a *C*-centred monoclinic unit cell with  $a = 16.8247(14)$  Å,  $b = 20.0177(17)$  Å,  $c = 9.9528(10)$  Å, and  $\beta = 106.190(10)^\circ$ . However, structure solution with this symmetry was not possible. Reduction to triclinic  $P\bar{1}$  symmetry allowed the structure to be solved and refined [Figure S3], although the *R* value remained above 10% at *R*=12%. The data was tested for twinning using Platon<sup>S3</sup> and the following twin matrix was identified

$$\begin{bmatrix} -1 & 0 & 0 \\ 0 & 0 & -1 \\ 0 & -1 & 0 \end{bmatrix}. \quad (\text{S1})$$

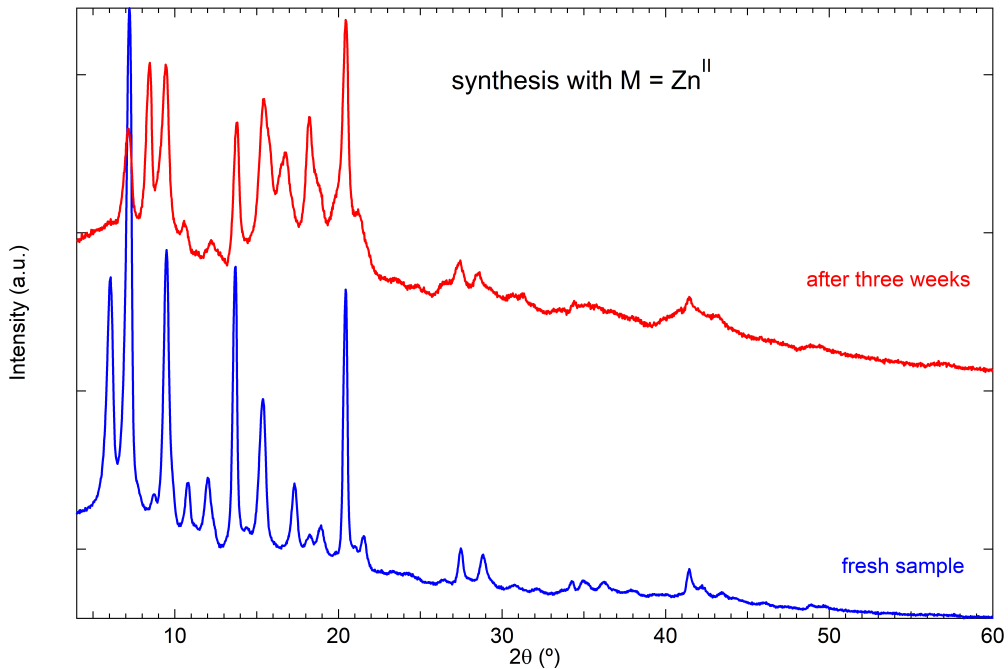


Figure S2: X-ray powder diffraction measured on the ambient powder of targeted  $\text{Zn}_2(2,6\text{-ndc})_2\text{dabco}$  synthesis (blue profile), and the same powder measured after three weeks exposed to air (red profile).

The inclusion of this twin matrix into the refinement gave a reduction in the  $R$  value to 7.2%.

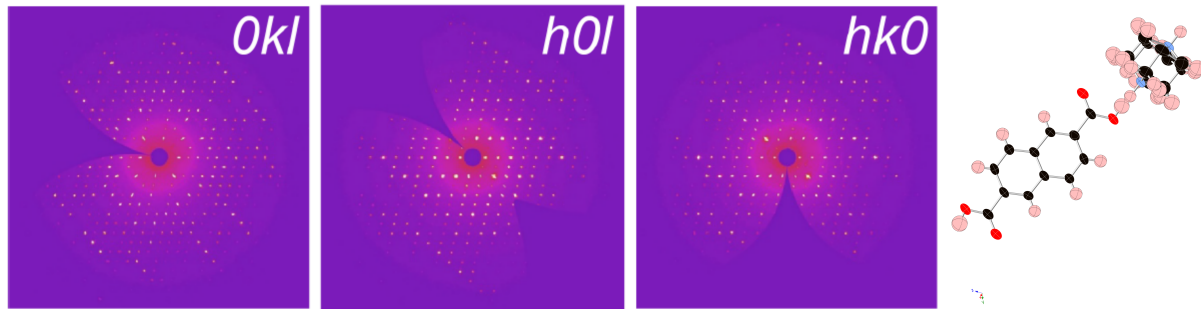


Figure S3: **Left)** (0kl), (h0l) and (hk0) planes, reconstructed from diffraction images of 2,6-ndc:dabco crystal **Right)** Structural unit of 2,6-ndc and dabco shown with 50% thermal ellipsoids. The hydrogens connecting 2,6-ndc and dabco are half occupied. The dabco ligand exhibits rotational disorder. Carbon atoms are represented in black, oxygen in red, nitrogen in blue and hydrogen in pink.

Table S1: Crystallographic details for (2,6-ndc):dabco crystal measured at ambient temperature.

Formula	C <sub>18</sub> H <sub>20</sub> N <sub>2</sub> O <sub>4</sub>
Crystal dimension ( $\mu\text{m}$ )	700 x 400 x 360
Crystal system	triclinic
Space group	<i>P</i> $\bar{1}$
Z	4
<i>a</i> ( $\text{\AA}$ )	9.9931(6)
<i>b</i> ( $\text{\AA}$ )	13.1049(6)
<i>c</i> ( $\text{\AA}$ )	13.1232(7)
$\alpha$ ( $^\circ$ )	99.940(4)
$\beta$ ( $^\circ$ )	100.300(5)
$\gamma$ ( $^\circ$ )	100.364(4)
<i>V</i> ( $\text{\AA}^3$ )	1625.65(16)
<b>Data collection</b>	
No. of reflections:	
measured	29088
unique	9119
unique with $I > 2 \sigma$	4612
R <sub>int</sub>	0.0795
<b>Refinement</b>	
No. of parameters	497
No. of restraints	124
R <sub>1</sub> [ $I > 2\sigma(I)$ ]	0.0723
wR <sub>2</sub> (all data)	0.1910
$\Delta\rho_{\max}, \Delta\rho_{\min}$ ( $e^- \text{\AA}^{-3}$ )	0.249 , -0.238

### 1.3 Ni<sub>2</sub>(2,6-ndc)<sub>2</sub>dabco

The ambient-temperature synthesis of DUT-8(Ni) yielded poorly crystalline and/or nanocrystalline powders as observed from X-ray powder diffraction [Figure S4].

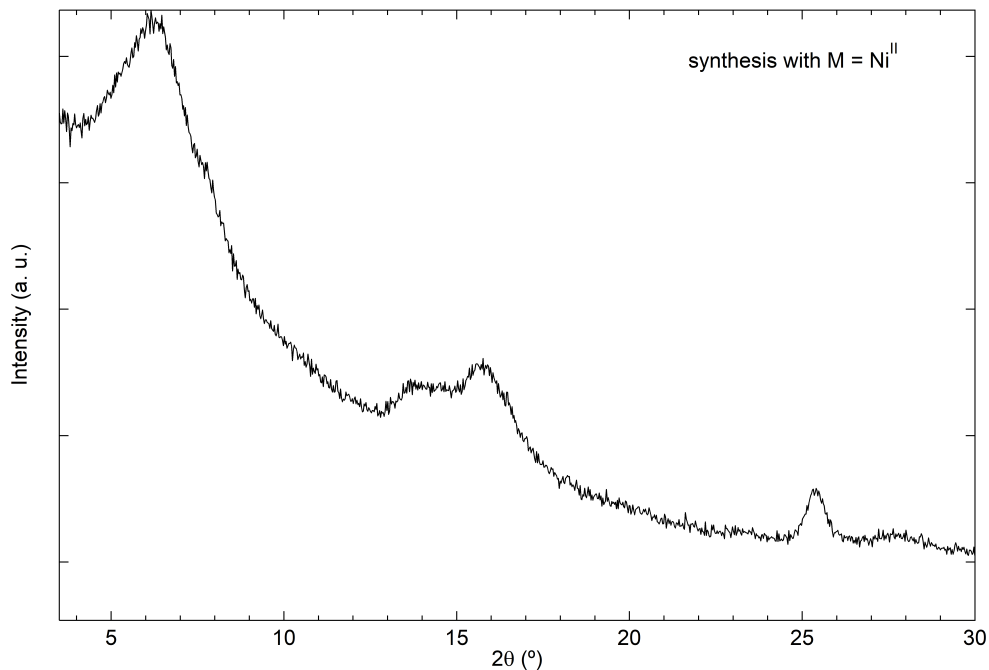


Figure S4: Powder X-ray diffraction from the targeted DUT-8(Ni)·3EtOH ambient-temperature synthesis in ethanol.

## 2 3D electron diffraction

### 2.1 Zn(2,6-ndc)(H<sub>2</sub>O)

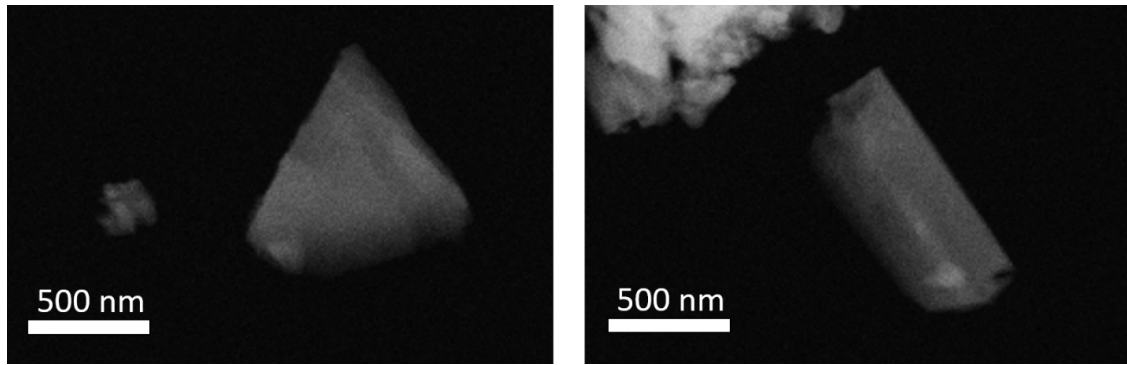


Figure S5: HAADF-STEM images of typical Zn(2,6-ndc)(H<sub>2</sub>O) crystals used for 3D ED data collections.

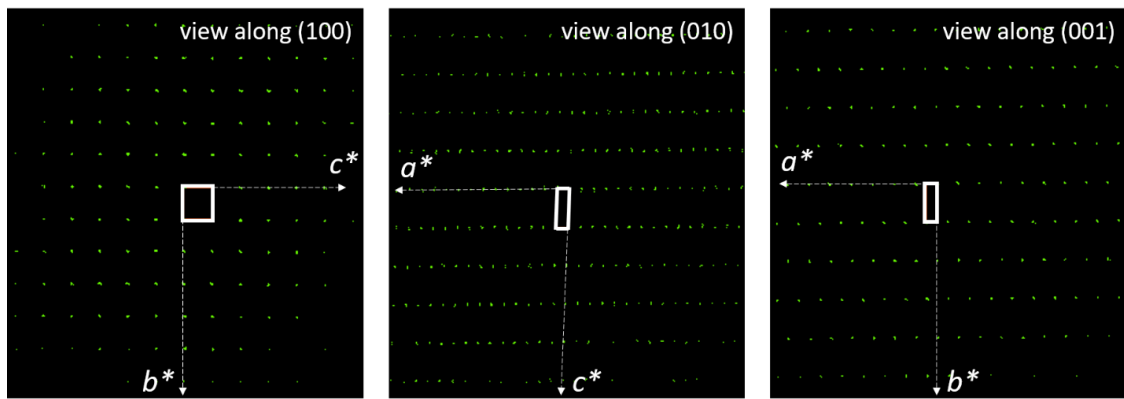


Figure S6: Reciprocal space from 3D ED data, viewed along the main crystallographic directions.

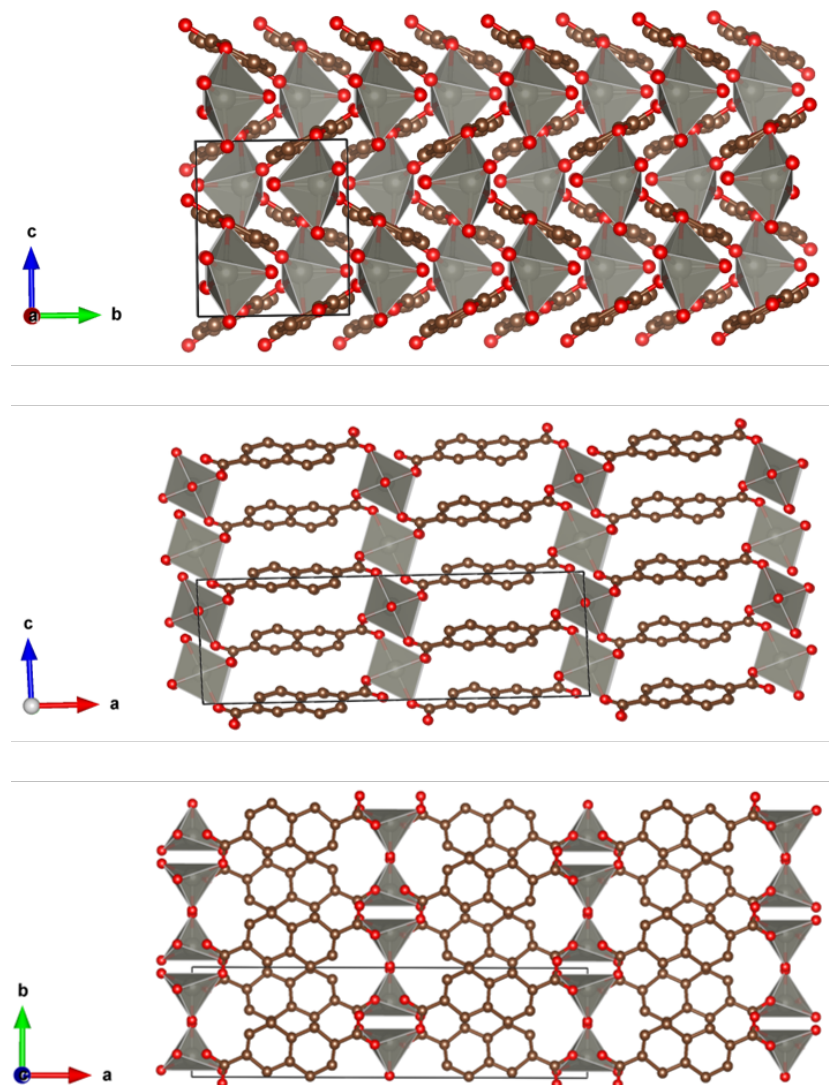


Figure S7: *Ab-initio* structural model of  $\text{Zn}(2,6\text{-ndc})(\text{H}_2\text{O})$ , as obtained after direct methods.

Table S2: Crystallographic details and atomic positions for Zn(2,6-ndc)(H<sub>2</sub>O), as determined from electron diffraction data.

Formula	Zn(2,6-ndc)(H <sub>2</sub> O)			
Space group	<i>C</i> 2/ <i>c</i>			
<i>a</i> (Å)	22.6936(17)			
<i>b</i> (Å)	6.3333(5)			
<i>c</i> (Å)	7.3027(7)			
$\alpha, \beta, \gamma$ (°)	90, 91.748(6), 90			
<i>Z</i>	8			
Atom	<i>x</i>	<i>y</i>	<i>z</i>	<i>U</i> <sub>iso</sub> (Å <sup>2</sup> )
Zn1	0.500000	0.6803(14)	0.250000	0.015(2)
O1	0.4215(7)	0.571(4)	0.172(2)	0.032(3)
O2	0.5372(8)	0.698(4)	-0.014(3)	0.032(3)
C1	0.5830(7)	0.6028(14)	-0.0739(7)	0.021(3)
C2	0.6406(4)	0.6855(8)	-0.0339(4)	0.021(3)
C3	0.6472(4)	0.8801(11)	0.0544(9)	0.021(3)
H3	0.614025	0.955921	0.087324	0.025
C4	0.7034(2)	0.9609(12)	0.0935(11)	0.021(3)
H4	0.707715	1.090504	0.152321	0.025
C5	0.74674(9)	0.6527(4)	-0.0442(4)	0.021(3)
C6	0.6905(2)	0.5719(9)	-0.0832(7)	0.021(3)
H6	0.686198	0.442333	-0.142042	0.025
O7	0.500000	0.977(7)	0.250000	0.048(7)
H7A	0.465880	1.050497	0.216245	0.057
H7B	0.534120	1.050497	0.283755	0.057

Table S3: Selected parameters from structure solution (SIR2014) and refinement (SHELXL) based on the 3D ED data.

Structure solution parameters (SIR2014)	
Data resolution ( $\text{\AA}$ )	0.8
No. of sampled reflections	2704
No. of independent reflections	760
Independent reflections coverage (%)	71
Global thermal factor $U_{\text{iso}}$ ( $\text{\AA}^2$ )	0.02226
$R_{\text{int}}(F)$ (%)	19.37
$R_{\text{SIR}}$ (%)	31.11
Structure refinement parameters (SHELXL)	
Data resolution ( $\text{\AA}$ )	0.8
$R_{\text{int}}(F^2)$ (%)	26.43
No. of reflections (all)	763
No. of reflections ( $> 4\sigma$ )	669
$R1 (> 4\sigma)$ (%)	33.37
$R1$ (all) (%)	34.94
Goodness-of-fit	3.954

## 2.2 Cu(2,6-ndc)

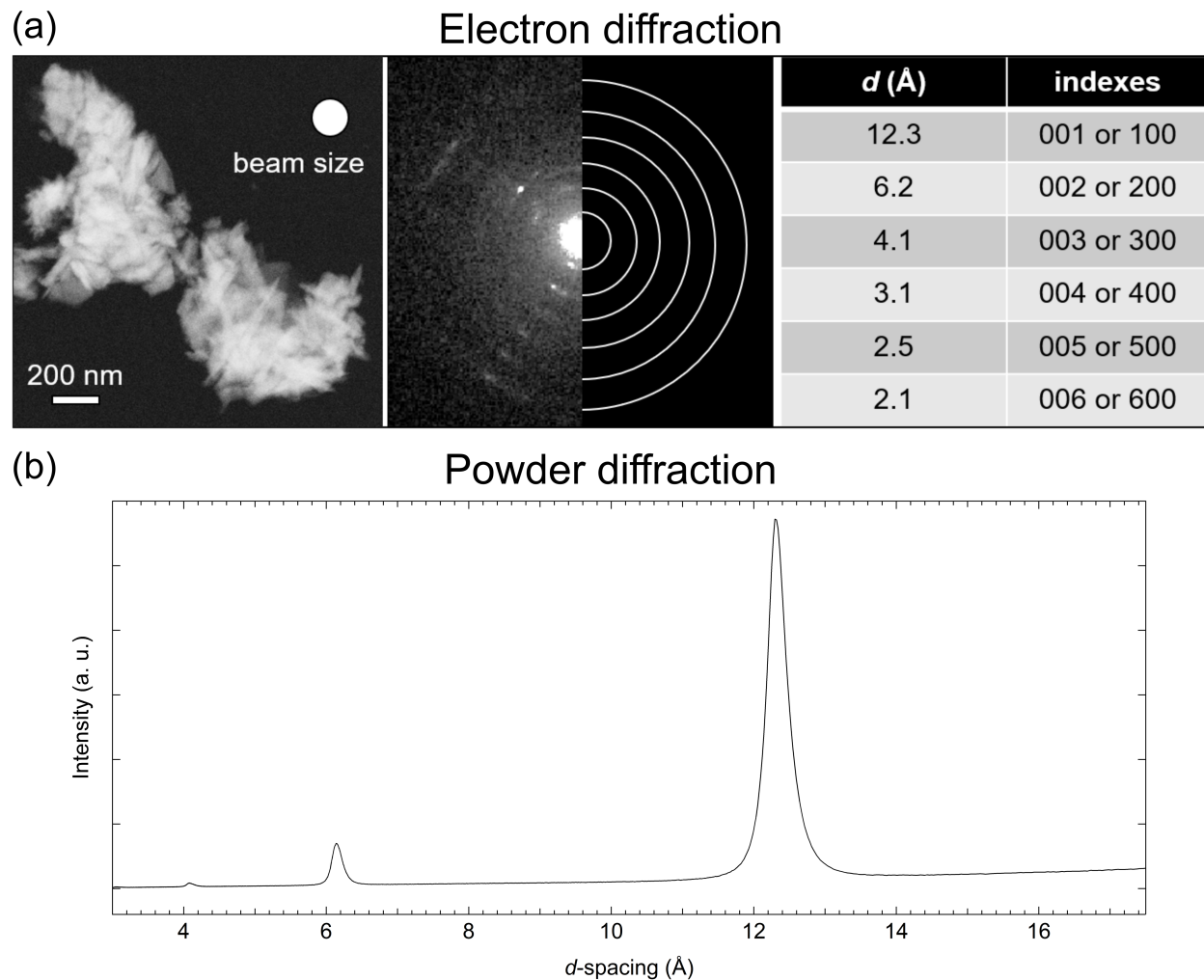


Figure S8: (a) HAADF-STEM image of typical Cu(2,6-ndc) crystals, with the raw ED pattern produced by an agglomerate of several nanocrystals. The detected  $d$ -spaces, corresponding to the  $h00$  and  $00l$  planes, are indicated in the table. (b) X-ray powder diffraction of the thin film of Cu(2,6-ndc) shown for comparison as a function of  $d$ -spacing.

### 3 Thin films

Table S4: Layer-by-layer thin film synthesis conditions with the metal salt (M with M = Cu<sup>2+</sup> or Zn<sup>2+</sup>) and ligand (L) concentrations, submersion times, and conditions given. Abbreviations for the SAMs: MHDA=16-mercaptohexadecanoic acid, PPMT = (4-(4-pyridyl)phenyl)methanethiol, PMBT = 4-(4-pyridyl)phenylmethylthiol, 4-MPA = 4-mercaptopbenzoic acid. Abbreviations for the ligands: bdc = 1,4-benzene dicarboxylate, 1,4-ndc = 1,4-naphthalene dicarboxylate, dabco = 1,4-diazabicyclo[2.2.2]octane, fu-bdc = functionalised-bdc such as 2,5-diethoxy-1,4-benzenedicarboxylate and 2,5-bis(2-methoxyethoxy)-1,4-benzenedicarboxylate, btc = benzene 1,3,5-tricarboxylate. RT = Room Temperature.

MOF	Concentration (mM)		Time (min)		Conditions	Ref.
	M	L	M	L		
M <sub>2</sub> (bdc) <sub>2</sub> (H <sub>2</sub> O) <sub>2</sub>	1	0.1	30	60	RT, MHDA, EtOH	4
M <sub>2</sub> (1,4-ndc) <sub>2</sub> (dabco)	2	0.2, 0.2	5	10, 10	40°C, MHDA, EtOH	5
Cu <sub>2</sub> (1,4-ndc) <sub>2</sub> (dabco)	1	0.1, 0.1	30	60, 10	RT, MHDA, EtOH	6
Zn <sub>2</sub> (bdc) <sub>2</sub> (dabco)	1	0.1, 0.1	30	60, 10	RT, MHDA, EtOH	6
Cu <sub>2</sub> (1,4-ndc) <sub>2</sub> (dabco)	0.5	0.2, 0.2	5	10, 10	40°C, MHDA, EtOH	7
Cu <sub>2</sub> (1,4-ndc) <sub>2</sub> (dabco)	0.5	0.2, 0.2	5	10, 10	40°C, PPMT, EtOH	7
Cu <sub>2</sub> (fu-bdc) <sub>2</sub> (dabco)	0.5	0.2, 0.2	10	10, 10	40°C, MHDA, EtOH	8
Cu <sub>2</sub> (fu-bdc) <sub>2</sub> (dabco)	0.5	0.2, 0.2	10	10, 10	40°C, PMBT, EtOH	8
Cu <sub>2</sub> (bdc) <sub>2</sub> (dabco)	2	0.2, 0.2	5	10, 10	40°C, 4-MBA, EtOH	9
Cu <sub>3</sub> (btc) <sub>2</sub> (H <sub>2</sub> O) <sub>n</sub>	1	1	30	60	RT, MHDA, EtOH	10
Cu <sub>3</sub> (btc) <sub>2</sub>	1	0.1	30	60	RT, MHDA, ETOH	11
Cu <sub>3</sub> (btc) <sub>2</sub>	1	0.1	3	5	RT, silica foam, EtOH	12

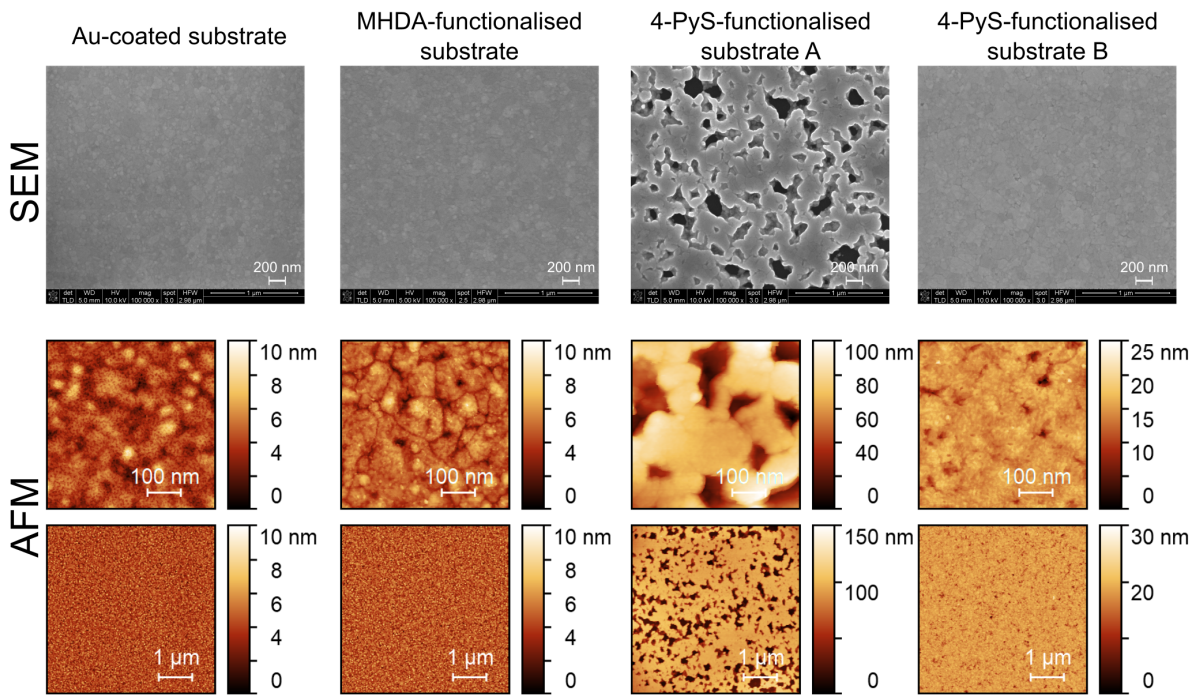


Figure S9: SEM and AFM images of Au-coated silicon substrate, MHDA-functionalised (20 mmol/L MHDA concentration) and 4-PyS-functionalised substrates. The A and B substrates represent 10 mmol/L and 0.1 mmol/L concentration of 4-Mercaptopyridine (4-PyS), respectively.

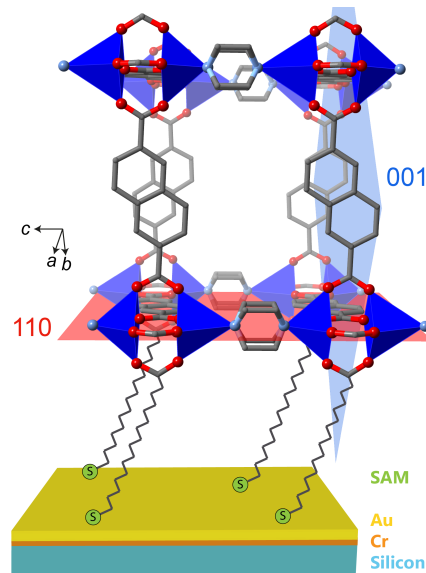


Figure S10: Schematic of the substrate, MHDA molecules, and the predicted (110) growth direction (red plane) of DUT-8. Through use of a pyridyl-terminated SAM, the growth direction along the (001) direction (blue plane) would also be feasible.

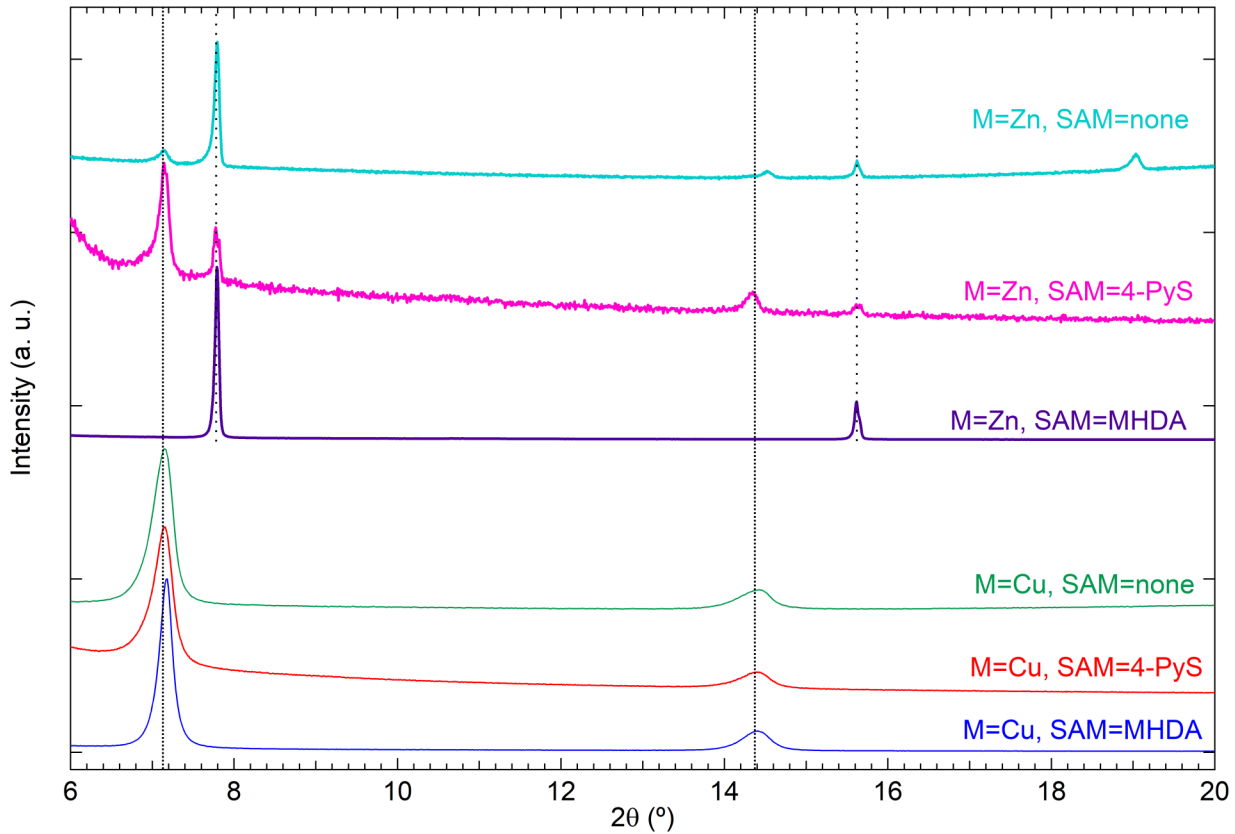


Figure S11: Powder X-ray diffraction patterns of the thin films when synthesised with  $M=Zn$  and  $M=Cu$  and different SAMs.

### 3.1 M=Zn, SAM=MHDA

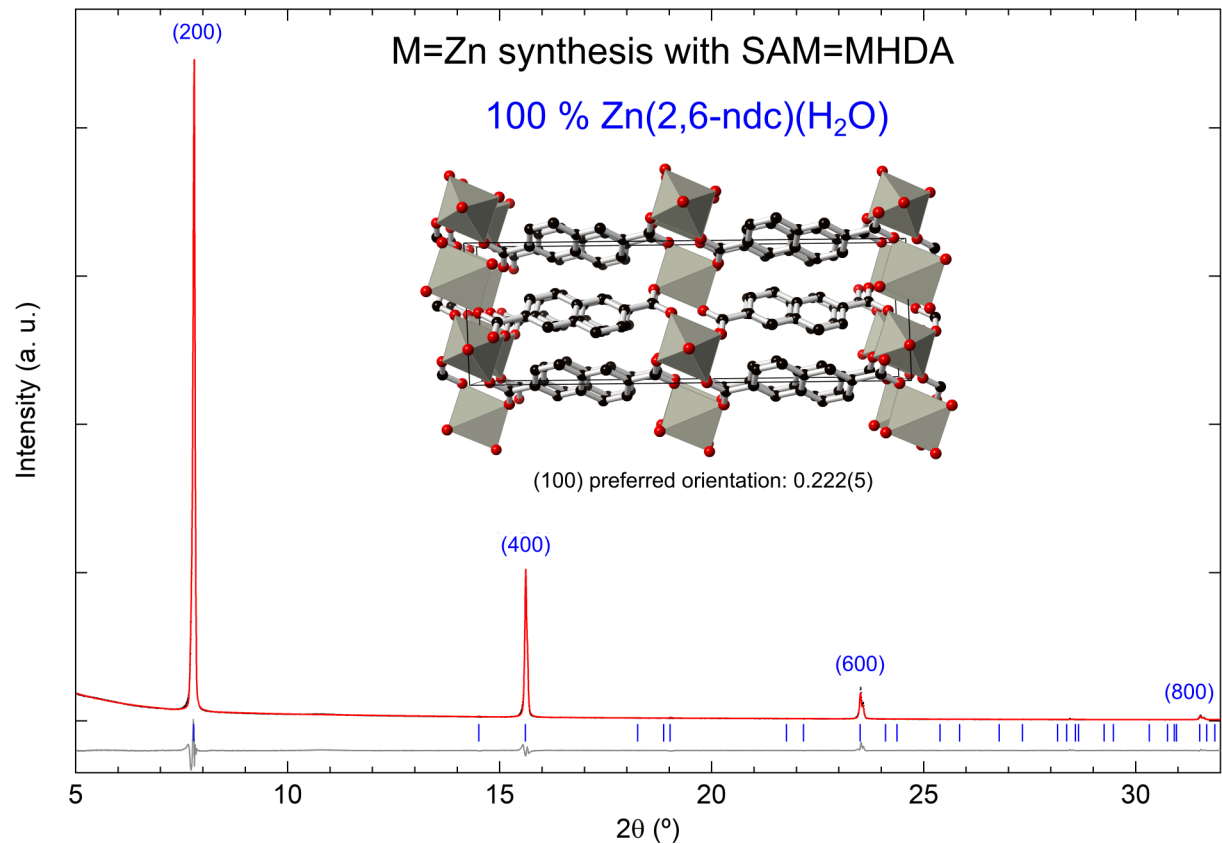


Figure S12: Rietveld fit of the  $\text{Zn}(2,6\text{-ndc})(\text{H}_2\text{O})$  structural model from Ref. 13 on the thin film X-ray powder diffraction pattern. Preferred orientation was refined using the March-Dollase factor along the (100) direction. Black points, red and grey lines represent the data, the fit, and the data-fit, respectively. The  $hkl$  tick marks are in blue. The structural model is shown as an inset.

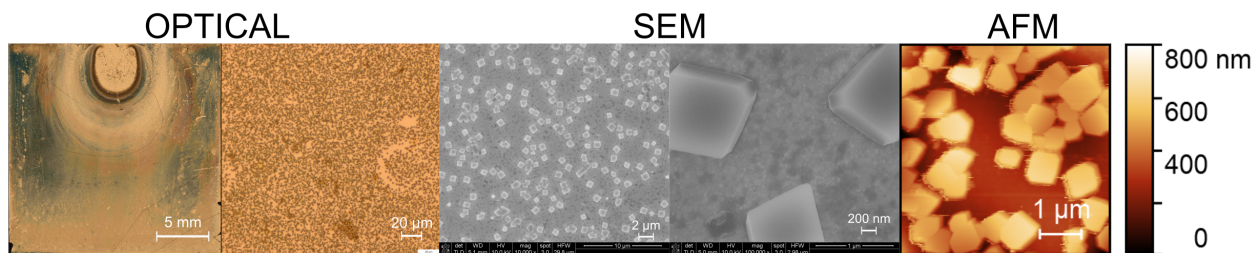


Figure S13: Optical, SEM, and AFM images of the  $\text{Zn}(2,6\text{-ndc})(\text{H}_2\text{O})$  thin film grown with MHDA as the SAM functionalisation.

### 3.2 M=Zn, SAM=4-PyS

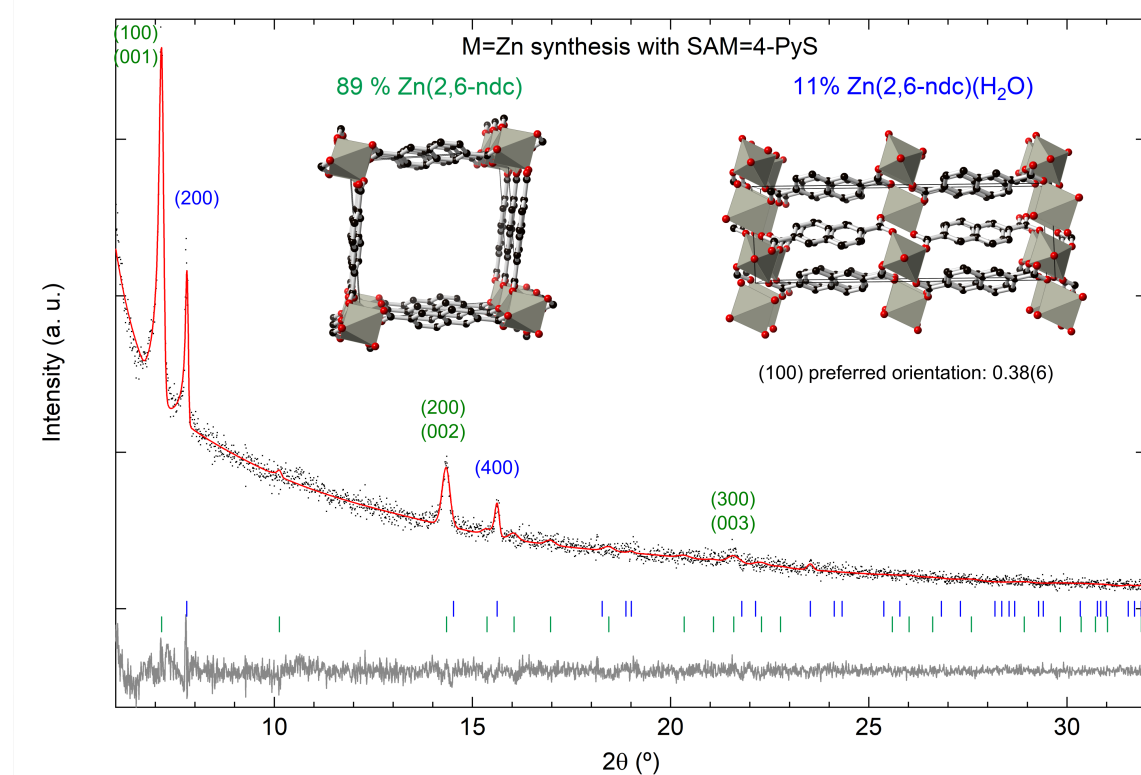


Figure S14: Rietveld fit of the M=Zn thin film synthesis with 4-PyS employed as SAM powder pattern using the Zn(2,6-ndc)(H<sub>2</sub>O) structural model from 3D electron diffraction and a Zn(2,6-ndc) model. Preferred orientation was refined using the March-Dollase factor along the (100) direction for the Zn(2,6-ndc)(H<sub>2</sub>O) phase. Black points, red and grey lines represent the data, the fit, and the data-fit, respectively. The *hkl* tick marks in blue and green represent the Zn(2,6)(H<sub>2</sub>O) and Zn(2,6-ndc) reflections, respectively.

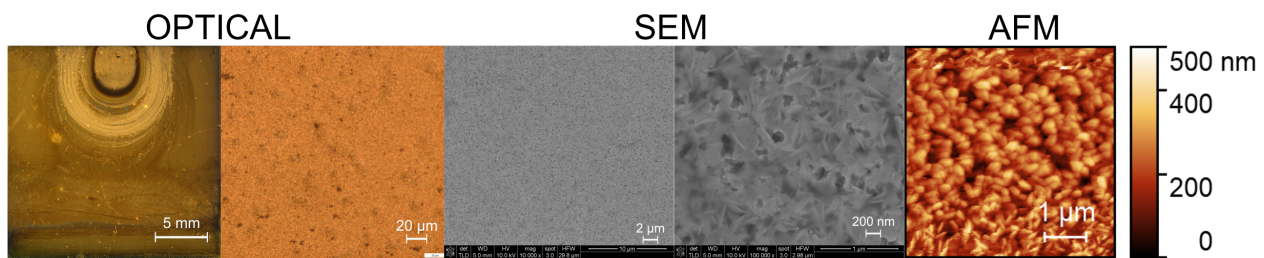


Figure S15: Optical, SEM, and AFM images of the Zn(2,6-ndc)(H<sub>2</sub>O) and Zn(2,6-ndc) thin film grown with 4-mercaptopypyridine as the SAM functionalisation.

### 3.3 M=Zn, SAM=none

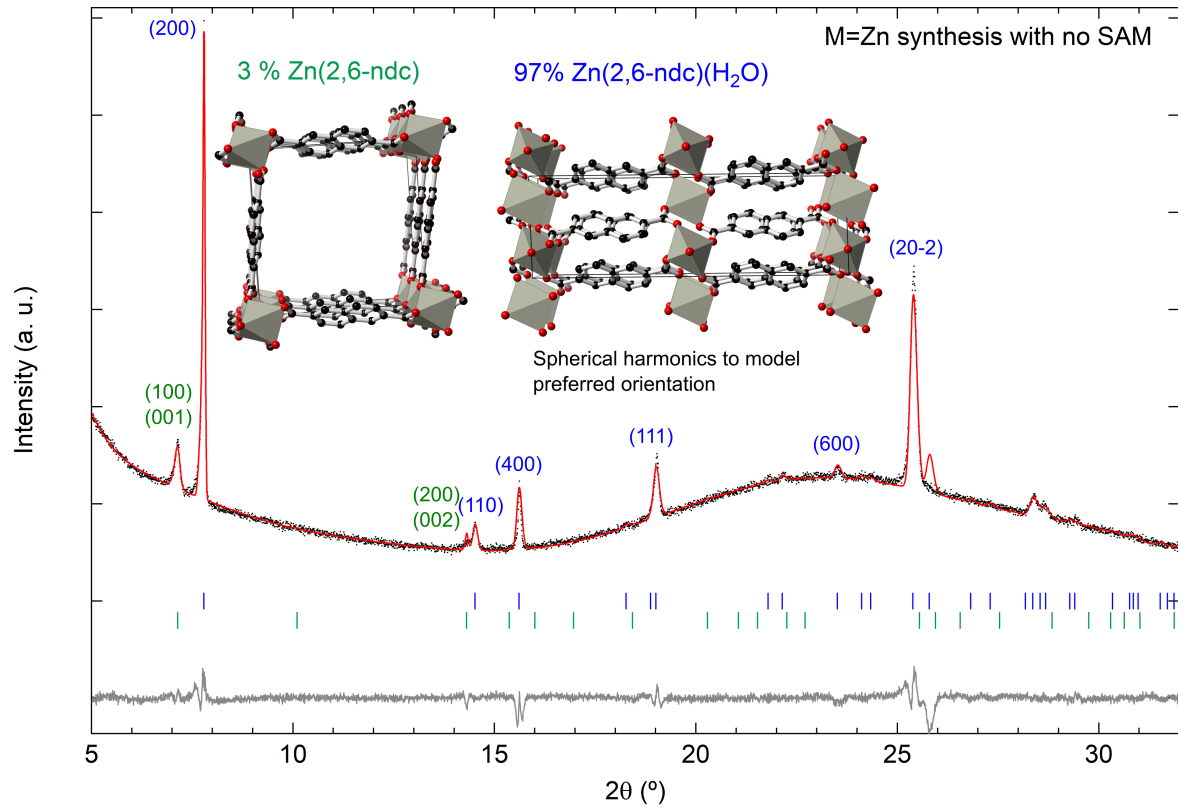


Figure S16: Rietveld fit of the M=Zn thin film synthesis on a glass slide with no SAM employed using the Zn(2,6)(H<sub>2</sub>O) structural model from 3D electron diffraction and a Zn(2,6-ndc) model. Black points, red and grey lines represent the data, the fit, and the data-fit, respectively. The  $hkl$  tick marks in blue and green represent the Zn(2,6-ndc)(H<sub>2</sub>O) and Zn(2,6-ndc) reflections, respectively. Spherical harmonics were used to model the preferred orientation of the Zn(2,6-ndc)(H<sub>2</sub>O) sample.

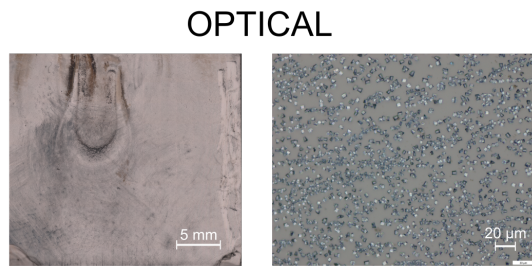


Figure S17: Optical images of the Zn(2,6-ndc)(H<sub>2</sub>O) crystals and Zn(2,6-ndc) phase grown on a glass slide with no SAM.

### 3.4 M=Cu, SAM=MHDA

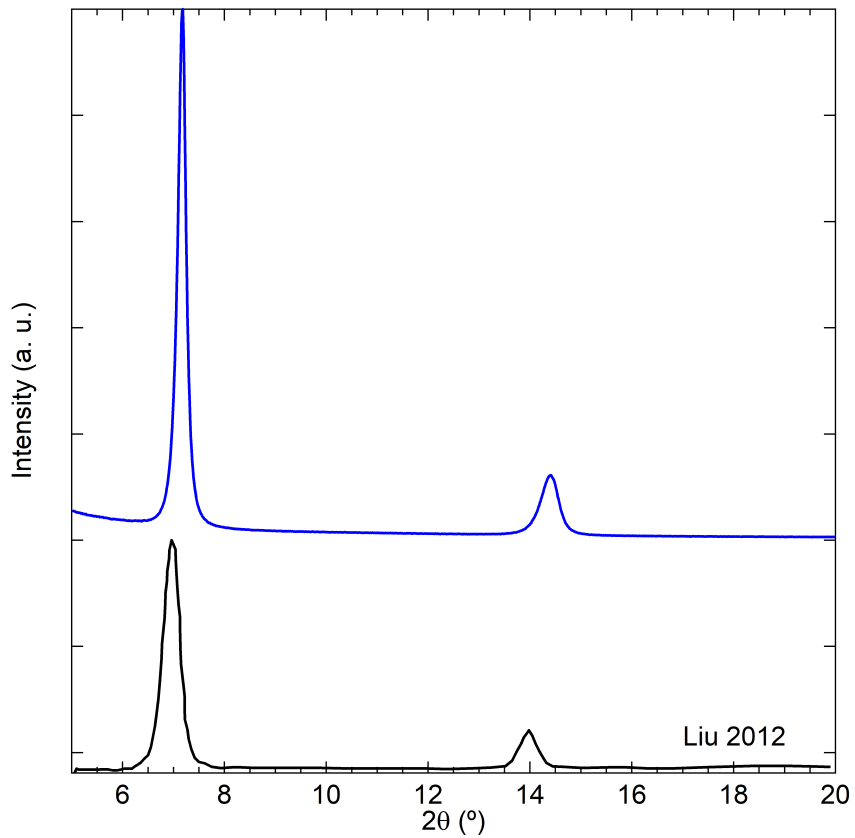


Figure S18: Powder X-ray diffraction patterns of the reported Cu(2,6-ndc) thin film from Ref. 14 (black pattern) and the thin film synthesised when M=Cu in this work (blue pattern).

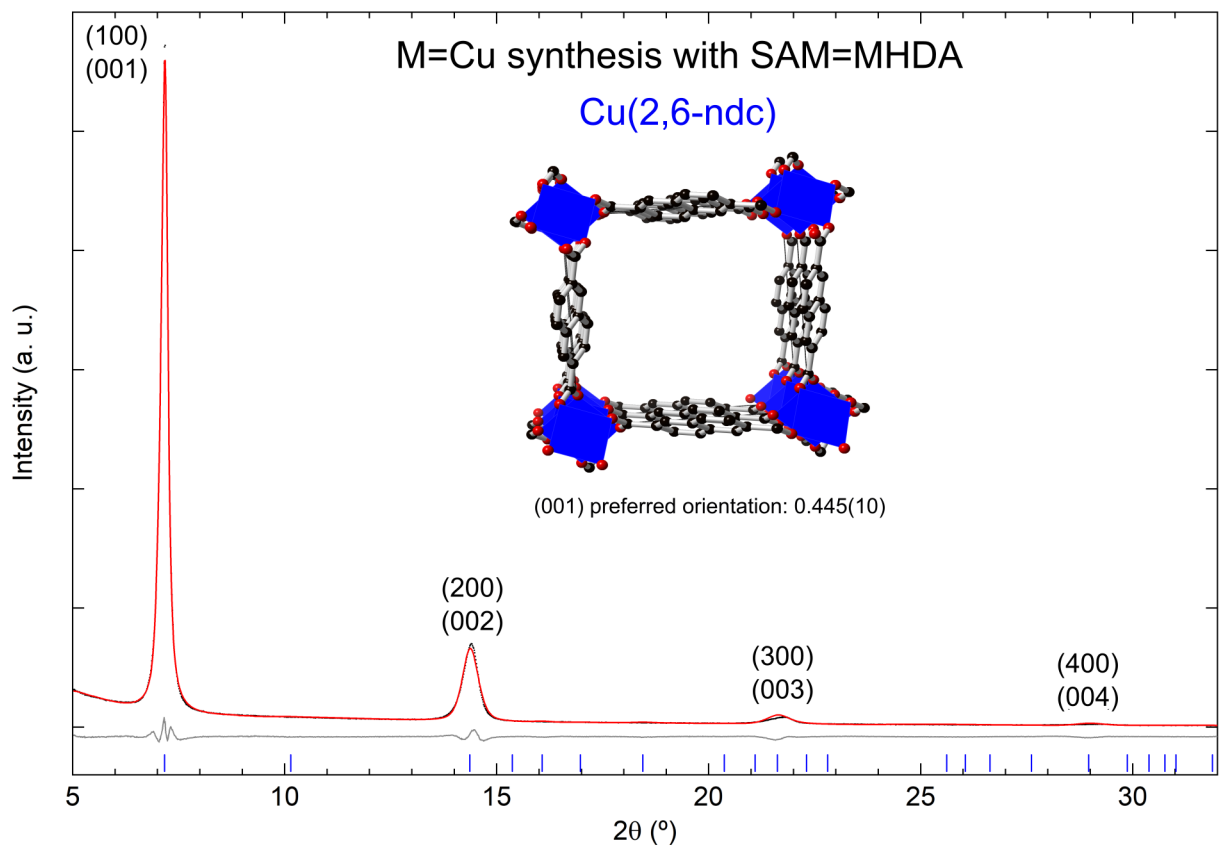


Figure S19: Rietveld fit of Cu(2,6-ndc) from the thin film synthesis with M=Cu and MHDA SAM used. Preferred orientation was refined using the March-Dollase factor along the (001) direction. Black points, red and grey lines represent the data, the fit, and the data-fit, respectively. The  $hkl$  tick marks are in blue. The structural model is shown as an inset.

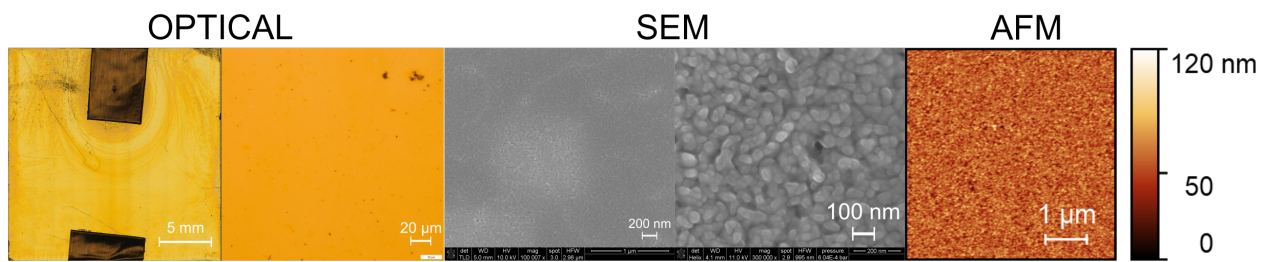


Figure S20: Optical, SEM, and AFM images of the Cu(2,6-ndc) thin film grown with MHDA as the SAM functionalisation.

Table S5: Crystallographic details and atomic positions for Cu(2,6-ndc), as refined from thin film powder diffraction data.

Formula	Cu(2,6-ndc)		
Space group	<i>P</i> 1		
<i>a</i> (Å)	12.3215(15)		
<i>b</i> (Å)	5.76103		
<i>c</i> (Å)	12.3215(15)		
$\alpha, \beta, \gamma$ (°)	90, 90, 90		
<i>R</i> <sub>wp</sub>	4.0%		
Atom	<i>x</i>	<i>y</i>	<i>z</i>
Cu1	0	0.185	0
Cu2	0	0.684	0
C1	0.467(11)	0.094(19)	0.023(7)
C2	0.357(7)	0.14(8)	0.044(15)
C3	0.31(2)	0.36(10)	0.021(14)
C4	0.38(4)	0.53(6)	-0.022(15)
C5	0.49(4)	0.488(12)	-0.043(15)
C6	0.533(10)	0.268(18)	-0.021(7)
C7	0.19(3)	0.41(17)	0.04(2)
O1	0.136(11)	0.3(2)	0.08(3)
O2	0.16(5)	0.60(19)	0.02(3)
C8	0.643(6)	0.22(8)	-0.042(15)
C9	0.69(2)	0.00(10)	-0.019(14)
C10	0.62(4)	-0.17(6)	0.024(15)
C11	0.51(4)	-0.125(12)	0.045(16)
C12	0.81(3)	-0.05(17)	-0.04(2)
O3	0.864(12)	0.1(2)	-0.08(3)
O4	0.84(5)	-0.23(19)	-0.02(3)
C13	-0.019(17)	0.090(17)	0.469(2)
C14	-0.042(19)	0.13(4)	0.359(4)
C15	-0.02(3)	0.34(2)	0.312(3)
C16	0.02(7)	0.526(15)	0.375(4)
C17	0.04(6)	0.49(3)	0.485(5)
C18	0.02(2)	0.273(19)	0.532(2)
C19	-0.05(4)	0.38(5)	0.191(5)
O5	-0.08(3)	0.23(8)	0.137(8)

O6	-0.03(7)	0.57(3)	0.150(5)
C20	0.04(2)	0.24(4)	0.642(4)
C21	0.03(3)	0.02(2)	0.689(3)
C22	-0.01(6)	-0.163(13)	0.626(3)
C23	-0.04(6)	-0.13(3)	0.516(5)
C24	0.05(4)	-0.02(5)	0.810(5)
O7	0.09(3)	0.14(8)	0.864(8)
O8	0.04(7)	-0.21(4)	0.851(5)

### 3.5 M=Cu, SAM=4-PyS

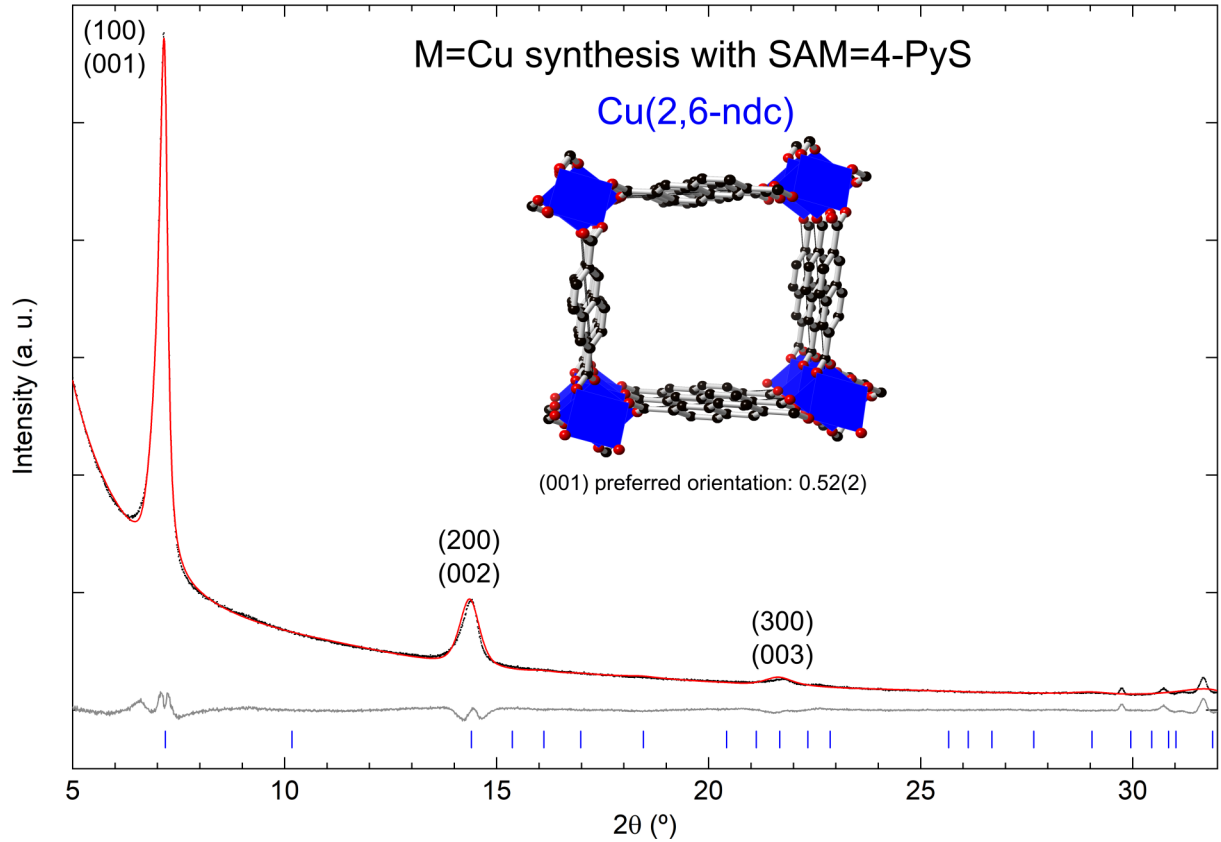


Figure S21: Rietveld fit of Cu(2,6-ndc) from the thin film synthesis with M=Cu and 4-PyS SAM used. Preferred orientation was refined using the March-Dollase factor along the (001) direction. Black points, red and grey lines represent the data, the fit, and the data-fit, respectively. The  $hkl$  tick marks are in blue. The structural model is shown as an inset

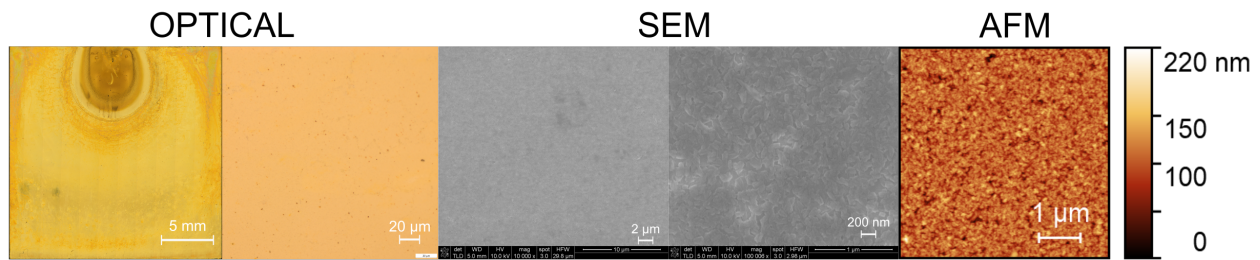


Figure S22: Optical, SEM, and AFM images of the Cu(2,6-ndc) thin film grown with 4-mercaptopypyridine as the SAM functionalisation.

### 3.6 M=Cu, SAM=none

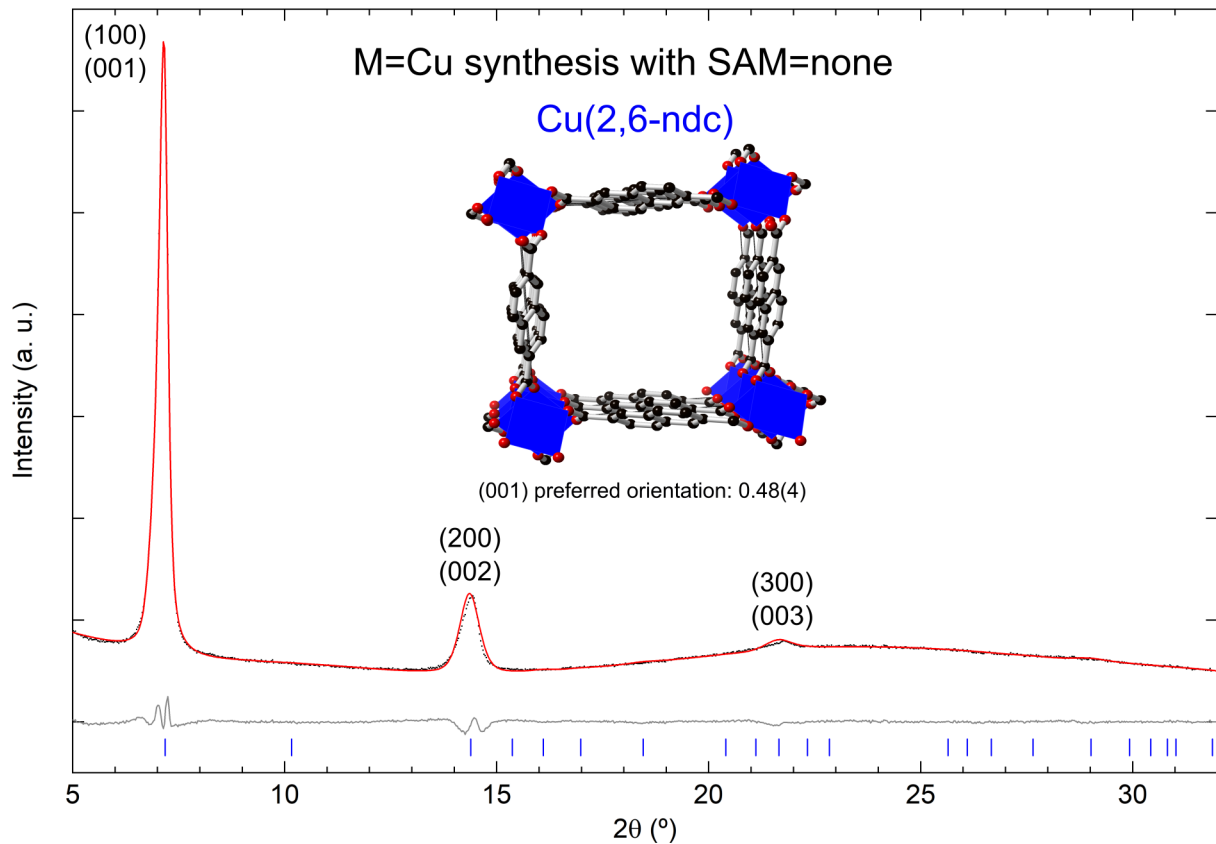


Figure S23: Rietveld fit of Cu(2,6-ndc) from the thin film synthesis with M=Cu and no SAM used. Preferred orientation was refined using the March-Dollase factor along the (001) direction. Black points, red and grey lines represent the data, the fit, and the data-fit, respectively. The *hkl* tick marks are in blue. The structural model is shown as an inset.

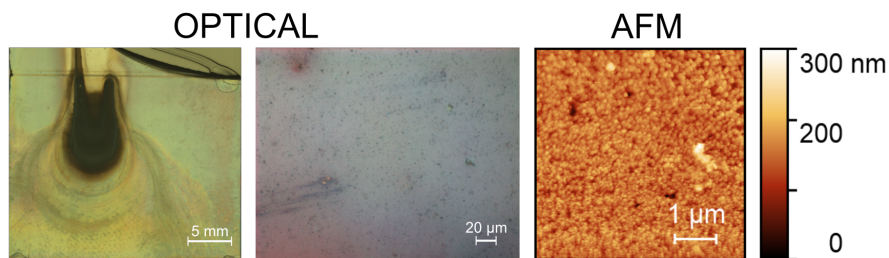


Figure S24: Optical and AFM images of the Cu(2,6-ndc) thin film grown on a glass slide with no SAM.

### 3.7 SEM thin film cross section

The thickness of the synthesised thin films could be estimated from the cross section SEM images. For these images, the operation voltage of 10 kV with a spot size of 3.5 was used, and the backscattered electron detector was additionally employed in order to obtain a greater phase contrast between the silicon substrate, gold layer and the synthesised thin film. For the Zn(2,6-ndc)(H<sub>2</sub>O) thin film (SAM=MHDA), the thickness could be estimated at 480(20) nm [Figure S25]. This value was taken from the average calculation of the four images shown in Figure S25, with the standard deviation indicating the error. The same analysis on the gold layer gave a thickness of 99(8) nm, which is consistent with the 100 nm layer deposited. In the case of the Cu(2,6-ndc) thin film (SAM=MHDA), it was much more sensitive to the electron beam, and thus proved difficult to image. One image using the backscattered electron detector indicates a thickness of 108 nm for the Au layer, and 166 nm for the Cu(2,6-ndc) layer [Figure S26].

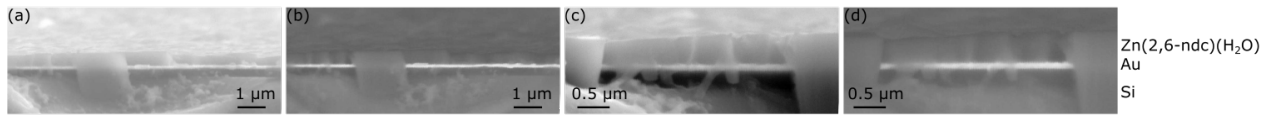


Figure S25: SEM cross section images of Zn(2,6-ndc)(H<sub>2</sub>O) thin film with images (a)/(b) or (c)/(d) taken at the same position. (a) and (c) images employed the Everhart-Thornley Detector (ETD) and (b) and (d) the backscattered electron detector (BSED).

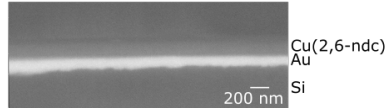


Figure S26: SEM cross section image of Cu(2,6-ndc) thin film employing the backscattered electron detector (BSED).

## References

- (S1) Klein, N.; Hoffmann, H. C.; Cadiau, A.; Getzschmann, J.; Lohe, M. R.; Paasch, S.; Heydenreich, T.; Adil, K.; Senkovska, I.; Brunner, E.; Kaskel, S. Structural flexibility and intrinsic dynamics in the M<sub>2</sub>(2,6-ndc)<sub>2</sub>(dabco) (M= Ni, Cu, Co, Zn) metal–organic frameworks. *J. Mater. Chem.* **2012**, *22*, 10303–10312.
- (S2) Abylgazina, L.; Senkovska, I.; Ehrling, S.; Bon, V.; Petkov, P. S.; Evans, J. D.; Krylova, S.; Krylov, A.; Kaskel, S. Tailoring adsorption induced switchability of a pillared layer MOF by crystal size engineering. *CrystEngComm* **2021**, *23*, 538–549.
- (S3) Spek, A. L. J. Single-crystal structure validation with the program PLATON. *J Appl Crystallogr* **2003**, *36*, 7–13.
- (S4) Arslan, H. K.; Shekhah, O.; Wieland, D. F.; Paulus, M.; Sternemann, C.; Schroer, M. A.; Tiemeyer, S.; Tolan, M.; Fischer, R. A.; Wöll, C. Intercalation in layered metal–organic frameworks: reversible inclusion of an extended  $\pi$ -system. *J. Am. Chem. Soc.* **2011**, *133*, 8158–8161.
- (S5) Zacher, D.; Yusenko, K.; Bétard, A.; Henke, S.; Molon, M.; Ladnorg, T.; Shekhah, O.; Schüpbach, B.; de los Arcos, T.; Krasnopolksi, M.; Meilikov, M.; Winter, J.; Terfort, A.; Wöll, C.; Fischer, R. A. Liquid-Phase Epitaxy of Multicomponent Layer-Based Porous Coordination Polymer Thin Films of [M(L)(P)0.5] Type: Importance of Deposition Sequence on the Oriented Growth. *Chem. Eur. J.* **2011**, *17*, 1448–1455.
- (S6) Shekhah, O. Layer-by-layer method for the synthesis and growth of surface mounted metal-organic frameworks (SURMOFs). *Materials* **2010**, *3*, 1302–1315.
- (S7) Liu, B.; Tu, M.; Fischer, R. A. Metal–Organic Framework Thin Films: Crystallite Orientation Dependent Adsorption. *Angew. Chem. Int. Ed.* **2013**, *52*, 3402–3405.
- (S8) Wannapaiboon, S.; Schneemann, A.; Hante, I.; Tu, M.; Epp, K.; Semrau, A. L.; Sternemann, C.; Paulus, M.; Baxter, S. J.; Kieslich, G.; Fischer, R. A. Control of structural flexibility of layered-pillared metal-organic frameworks anchored at surfaces. *Nat. Commun.* **2019**, *10*, 346.
- (S9) Hase, M.; Chun, W.-J.; Kondo, T. Layer-by-Layer Construction of Three-Dimensional MOF [Cu<sub>2</sub>(bdc)<sub>2</sub>dabco]<sub>n</sub> on Au Surface. *ECS Transactions* **2017**, *75*, 49.
- (S10) Shekhah, O.; Wang, H.; Kowarik, S.; Schreiber, F.; Paulus, M.; Tolan, M.; Sternemann, C.; Evers, F.; Zacher, D.; Fischer, R. A.; Wöll, C. Step-by-step route for the synthesis of metal-organic frameworks. *J. Am. Chem. Soc.* **2007**, *129*, 15118–15119.
- (S11) Shekhah, O.; Wang, H.; Zacher, D.; Fischer, R. A.; Wöll, C. Growth mechanism of metal-organic frameworks: Insights into the nucleation by employing a step-by-step route. *Angew. Chem. Int. Ed.* **2009**, *48*, 5038–5041.
- (S12) Shekhah, O.; Fu, L.; Sougrat, R.; Belmabkhout, Y.; Cairns, A. J.; Giannelis, E. P.; Eddaoudi, M. Successful implementation of the stepwise layer-by-layer growth of MOF thin films on confined surfaces: mesoporous silica foam as a first case study. *Chem. Commun.* **2012**, *48*, 11434–11436.
- (S13) Min, D. W.; Yun, S. S.; Lee, C. U.; Lee, C. Y.; Seo, M. G.; Hwang, Y. J.; Han, W. S.; Lee, S. W. A zinc (II)-carboxylate coordination polymer constructed from zinc nitrate and 2,6-naphthalenedicarboxylate. *Bull. Korean Chem. Soc.* **2001**, *22*, 531–533.
- (S14) Liu, J.; Lukose, B.; Shekhah, O.; Arslan, H. K.; Weidler, P.; Gliemann, H.; Bräse, S.; Grosjean, S.; Godt, A.; Feng, X.; Müllen, K.; Magdau, I.-B.; Heine, T.; Wöll, C. A novel series of isoreticular metal organic frameworks: realizing metastable structures by liquid phase epitaxy. *Sci Rep* **2012**, *2*, 921.